Just Add Ligands: Self-Sustained Size Focusing of Colloidal Semiconductor Nanocrystals.

Natalia Razgoniaeva[1,2], Mingrui Yang[1,2], Paul Garrett[3], Natalia Kholmicheva[1,2], Pavel Moroz[1,2], Holly Eckard[4], Luis Royo Romero[2], Dmitry Porotnikov[1,2], Dmitriy Khon[3], Mikhail Zamkov[1,2].*

The Center for Photochemical Sciences[1], Department of Physics[2] and Department of Chemistry[4] Bowling Green State University, Bowling Green, Ohio 43403. Department of Chemistry and Biochemistry[3], St. Mary's University, San Antonio, Texas, 78228.

Corresponding author: zamkovm@bgsu.edu; Tel: 419-372-0264; Fax: 419-372-9938

RECEIVED DATE (to be automatically inserted after your manuscript is accepted if required)

Abstract. Digestive ripening (DR) represents a powerful strategy for improving the size homogeneity of colloidal nanostructures. It relies on the ligand-mediated dissolution of larger nanoparticles in favor of smaller ones and is often considered to be the opposite of Ostwald ripening. Despite its successful application to size-focusing of metal colloids, digestive ripening of semiconductor nanocrystals has received little attention to date. Here, we explore this synthetic niche and demonstrate that ligand-induced ripening of semiconductor nanocrystals

exhibits an unusual reaction path. The unique aspect of the DR process in semiconductors lies in the thermally activated particle coalescence, which leads to a significant increase in the nanocrystal size for temperatures above the threshold value (T_{th}=200-220 ˚C). Below this temperature, nanoparticle sizes focus to an ensemble average diameter just like in the case of metal colloids. The existence of the thermal threshold for coalescence offers an expedient strategy for controlling both the particle size and the size dispersion. Such advanced shape control was demonstrated using colloids of CdS, CdSe, $CsPbBr_3$, and $CuZnSnS_4$ semiconductors, where monodisperse samples were obtained across broad diameter ranges. We expect the demonstrated approach to be extended to other semiconductors as a simple strategy for tuning the nanoparticle morphology.

INTRODUCTION

The synthesis of colloidal semiconductor nanocrystals (NCs) has been continuously perfected over the course of several decades.[1-3] The primary goal behind these synthetic efforts was aimed at achieving a narrow distribution of nanoparticle sizes, which pertains to many useful characteristics of colloidal nanocrystals and their solids.[4-10] For instance, the low dispersion of nanocrystal shapes can facilitate the assembly of inorganic colloids into superlattices[11] or reduce the dispersion of excited state energies across the film.[12] The fundamental advances resulting from an improved particle homogeneity could be harnessed towards diverse applications, including enhancing the color purity in light-emitting applications,[13,14] increasing the charge extraction efficiency in photovoltaic devices,[15-17,] or processing of nanocrystals into long-range ordered solids exhibiting excitonic bands.[18]

Controlling the nucleation rate has been recognized as one of the most effective tools for achieving a narrow distribution of nanoparticle sizes during growth.[19,20] At the current state of the art, hot injection strategies can be used to obtain nanocrystal samples with the standard size deviation within a 5-10%[4,21,22] range, which could be further reduced through the size-selective precipitation techniques.[23-25] It is, however, a highly parametrized strategy that requires timing the precursor decomposition to achieve size focusing.[21,26-32] In addition to nucleation-based approaches, a narrow 3-5% particle size dispersion was recently realized[33] through a sequential application of the colloidal atomic layer (c-ALD)[34] deposition for a stepwise synthesis of half-monolayers. This method, however, required a rather laborious synthetic protocol.

Considering the complex nature of hot-injection strategies, post-synthetic treatments have been developed as alternative methods for improving the particle homogeneity.[31] Among those, digestive ripening (DR) has emerged a facile strategy for narrowing the size distribution of metal colloids. First proposed in 2000 by Lin, Sorensen, and Klabunde,[35] the DR process is typically initiated by the addition of free ligand molecules to the nanoparticle solution at a relatively high concentration and is catalyzed by the application of heat.[36,37] The increase in the solvent temperature results in a ligand-mediated dissolution of larger-diameter nanocrystals, which leads to size focusing. In this regard, the DR mechanism is sometimes viewed as being opposite to the processes of Ostwald ripening,[38] where small particles, placed in a ligand-deprived environment, dissolve in favor of larger ones. Thus far, the DR method has been successfully applied to narrowing the size dispersion of many metal colloids, including Au,[39,40] Ag,[41] Cu,[42] Ru,[43] as well as metal oxides[44] and semiconductor clusters.[45] The application of digesting ripening to

semiconductor nanocrystal colloids, however, has been limited to few early papers[46,47] that reported an improved size dispersion in treated CdSe NCs.

Here, we demonstrate that ligand-mediated digestive ripening of semiconductor nanocrystals can be used to control both the average particle size and the ensuing size dispersion. In contrast to the size-focusing mechanism of metal nanoparticles, the digestive ripening of semiconductor nanocrystals was found to be accompanied by a significant increase in the average particle diameter at temperatures above a certain thermal threshold, T_{th} = 200-220 ˚C. A set of control experiments have confirmed that such behavior was the result of two competing processes that included particle coalescence and the concurrent size focusing.[48] Both reactions were initiated by the addition of free ligand molecules, such as oleylamine (OLAM) or oleic acid (OA) to nanocrystal solutions at 160-260 ˚C, which promoted ion solubility and interparticle monomer exchange. Notably, the coalescence process was prevalent only if the reaction temperature was greater than T_{th}. The existence of such an activation threshold for a particle coalescence allowed controlling the ultimate size of semiconductor nanocrystals through the DR treatment; a functionality not easily available in the case of metal nanoparticles.[49] In this work, the digestive ripening approach was demonstrated for CdS, CdSe, $CsPbBr_3$, and $CuSnZnS_4$ semiconductor nanocrystals. We expect the demonstrated strategy could be extended to other semiconductor materials as a simple tool for adjusting the average particle size and reducing the particle diameter dispersion in colloidal nanocrystal solutions.

EXPERIMENTAL SECTION

Materials. Cadmium oxide (CdO, 99.5% Aldrich), 1-octadecene (ODE, 90% Aldrich), oleic acid (OA, 90% Aldrich), sulfur (S, 99.999% Acros), methanol (anhydrous, 99.8% Aldrich), chloroform (anhydrous, 99% Aldrich), copper (II) acetylacetonate (99.99% Aldrich), zinc chloride (≥98% Aldrich), tin (II) acetate(Aldrich), oleylamine (OLAM, tech., 70% Aldrich), hexane (anhydrous, 95% Aldrich), ethanol (anhydrous, 95% Aldrich), isopropyl alcohol (99.9% Omnisolv), tri-n-octylphosphine oxide (TOPO, 99.0% Aldrich), selenium powder (Se, 200 mesh, Acros), cesium carbonate ($CsCO_3$, 99.5% Acros), lead (II) bromide ($PbBr_2$, 98+% Acros), acetone (anhydrous, Amresco, ACS grade), stearic acid (97% Aldrich), tributylphosphine (TBP, 97% Aldrich).

Synthesis of CdS NCs. CdS NCs were fabricated according to the previously reported procedure.[50] A mixture of 0.0768 g (0.6 mmol) of CdO, 3.6 mL of OA, and 24 mL of ODE in a 50 mL three-neck flask was heated to 240 °C until the solution turned optically clear and colorless. Then, the mixture was allowed to stir at this temperature at which point all of the sulfur precursor solution made by dissolving 0.02 g (0.625 mmol) of sulfur powder at 200 °C in ODE (10 mL) was quickly injected. The reaction was stopped by removing the flask from the heating mantle after 4−5 min. CdS NCs were separated from the solution by precipitating with methanol and redissolving the product in chloroform.

Synthesis of $CuZnSnS_4$ NCs. The $CuZnSnS_4$ NCs were obtained using a procedure by Collord.[51] A mixture of 0.362g (1.37mmol) copper (II) acetylacetonate, 0.19g (0.865mmol) zinc chloride, 0.263g (0.75mmol) tin (II) acetate, and 11 mL of oleylamine was added to a three-neck flask, degassed at 130°C for 1 hour, cycling to atmospheric pressure with argon every 20 min and re-pumping down. After degassing, the solution was heated to 225°C and 4mL of 1M sulfur in OLAM solution was injected. The reaction was stopped by removing the flask from the heating mantle after a set reaction time. The product was transferred to several centrifuge tubes. 4 ml of hexane and 4 ml of ethanol were added to each test tube, the solutions were centrifuged for 5 min and the supernatant was separated. The supernatant was split into 2 tubes, topped with 2 ml of hexane and 12 ml of isopropyl alcohol (each tube) and then centrifuged one more time followed by redissolution in hexane.

Synthesis of CdSe NCs. CdSe NCs were prepared using a previously reported strategy.[52] In a three-neck flask, stearic acid (0.67 g), ODE (7.1 mL), and CdO (0.078 g) were heated to 200 °C

under argon atmosphere until the solution turned clear. Once the reaction mixture was allowed to cool to room temperature, 4.5 g of ODA and 1.5 g of TOPO were added. The flask was reheated to 280 °C under vigorous stirring, and selenium solution, prepared under argon by dissolving 0.461 g of selenium powder *via* sonication in TBP (2 mL) and further diluting it with 5.2 mL of ODE, was quickly injected. The temperature was set at 250 °C, and the reaction continued until the absorption peak was red-shifted to $\lambda \approx 600$ nm, at which point the reaction was quenched by removing the flask from the heating mantle. Once the flask's contents had cooled to 60 °C, 10 mL of chloroform was injected into the flask to prevent solidification. To remove the unreacted material, the contents of the flask were centrifuged and the precipitate was discarded. Acetone (6 mL) was added to the supernatant, and the solution was centrifuged again. The final precipitate was stored in chloroform.

Synthesis of $CsPbBr_3$ nanocrystals. $CsPbBr_3$ nanocrystals we fabricated according to the protocol developed by Protosescu et al.[53] In a typical synthesis, a mixture of $PbBr_2$ (0.069g), ODE (5 mL), OA (0.5 mL) and OLAM (0.5 mL) was degassed at 120°C for 1 hour, then switched to argon and heated to 200°C to dissolve the $PbBr_2$ salt. The solution was kept at 200°C until the injection of Cs precursor. Separately, in a 10 mL flask, 0.0814g $CsCO_3$, 4 mL ODE and 0.25 mL OA were degassed at 120°C for 1 hour, then switched to argon atmosphere and heated up to 150°C until all the $CsCO_3$ reacted with oleic acid. Then, the temperature was decreased to 100°C and 0.4 mL of Cs-oleate solution was quickly transferred into the first flask. The reaction was stopped after 5 sec by removing the flask from the heating mantle and placing it into a water bath. The nanocrystals were isolated from the mixture by precipitating with butanol, centrifuging, and redispersing in hexane.

Digesting ripening of semiconductor nanocrystals. The original nanocrystal seeds (CdS, CdSe, $CsPbBr_3$, or $CuZnSnS_4$) were transferred into a flask containing a desired ligand (OLAM, OA)/solvent (ODE) combination (total volume is 7ml) and degassed to remove the chloroform or hexane. The reaction mixture was subsequently heated to 160 - 260°C under argon. When the original nanocrystal seeds reached the desired size, the reaction was stopped by removing the flask from the heating mantle. The NC product was separated from the solution by precipitation with ethanol (semiconductor nanocrystals) or butanol (perovskites) and redispersion in chloroform or hexane (perovskites).

Characterization. UV-vis absorption spectra were recorded using a CARY 60 scan spectrophotometer. High-resolution transmission electron microscopy (TEM) measurements

were carried out using JEOL 311UHR operated at 300 kV. Specimens were prepared by depositing a drop of NP solution in an organic solvent onto a carbon-coated copper grid and allowing it to dry in air. Powder X-Ray diffraction measurements were carried out with a Bruker D8 Advance PXRD.

RESULTS AND DISCUSSIONS

In the case of metal nanoparticles, digestive ripening is usually initiated with the addition of ion-solubilizing ligand molecules into the reaction solvent, such as toluene or octadecene. In a ligand-rich environment, nanocrystals attain an enhanced level of fluidity that allows annealing and rearrangement of lattice atoms.[49] These processes are catalyzed by heating the solution to 60-120 ˚C, which preferentially affects small-diameter nanoparticles featuring lower melting temperatures compared to their bulk.[54] Refluxing of the reaction mixture for several hours results in reshaping of nanoparticles toward a narrower size distribution. Previous works[55-57] highlighted the key role of free ligands in enhancing the rate of nanoparticle shape transformations. The analysis of the crystal structure in Au clusters that were subjected to the DR process in the presence of a p-mercaptobenzoic acid ligand has indicated that stable Au-Au bonds become replaced with Au-S-Au.[55] The inserted sulfur atoms can then etch the Au surface causing the formation of Au_xS_y islands,[57] which are transported away from the host surface. The mobility of ions and small clusters in solution drives the nanoparticle growth towards minimizing the ensample total surface area. In the case of metal nanoparticles, this results in narrowing of the diameter distribution without a significant increase in the particle size. A moderate, < 50% increase in the average particle size, however, could be induced through the use of long-chain ligands (e.g. dodecanethiol) promoting particle coalescence and the formation of bimodal structures.[58]

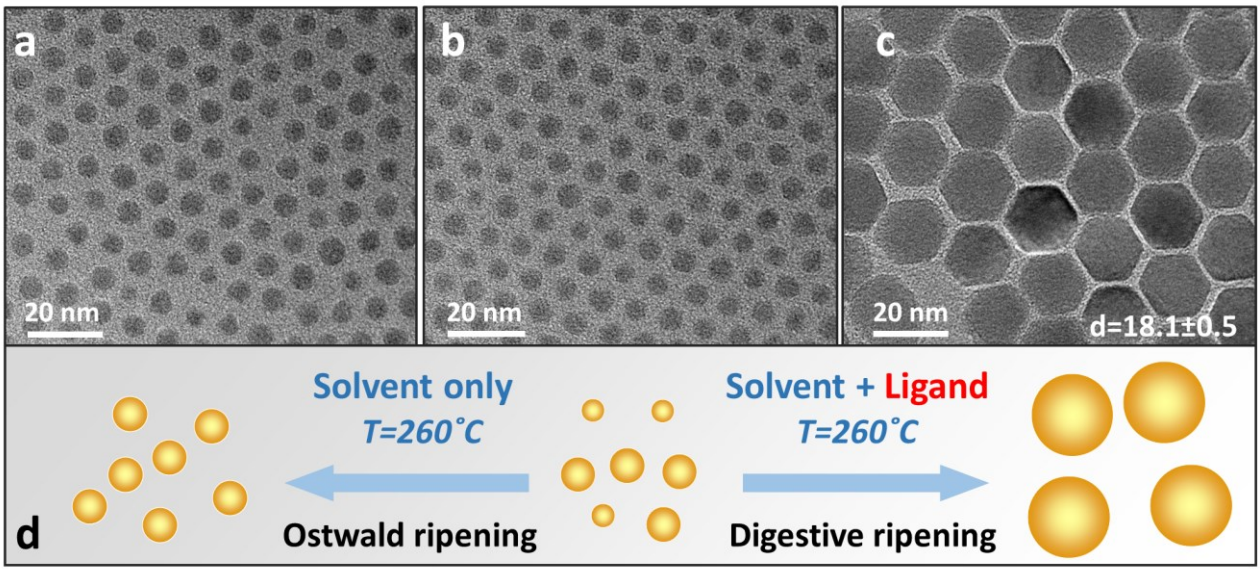

Figure 1. Illustration of the digestive ripening process in samples of CdS semiconductor nanocrystals. (a). A Transmission Electron Microscopy (TEM) image of a control sample of CdS NCs after heating the original 4.6-nm CdS seeds for 7 hours in octadecene (no ligands were added). A minor 4.6 nm → 4.7 nm size increase was observed. (b) TEM image of the original CdS NC sample prior to heating. (c). TEM image of CdS NC after heating for 4 hours in the presence of oleylamine ligand (OLAM:ODE = 60:40). A significant size growth was attributed to digestive ripening. (d). A scheme summarizing the differences between digestive and Ostwald ripening processes.

In light of the limited literature available on the DR process in semiconductor colloids, we have chosen to explore the fundamental effects of ligand-mediated ripening in well-investigated examples of semiconductor NCs, including cadmium chalcogenides and $CuZnSnS_4$ (CZTS) quantum dots. 4.6-nm CdS NCs featuring size distribution of ≈ 6% were investigated first (Fig. 1b). To this end, as prepared nanoparticles were cleaned and reloaded into a flask containing an octadecene (ODE) solvent. Without the addition of free ligands, heating of the

reaction mixture to 260 ˚C did not produce significant changes in the nanoparticle shape even after several hours (see Figs. 1a and SF1). Some mild size increase, tentatively attributed to Ostwald ripening, could be observed after 7 hours of heating (see Fig. SF5 for size histograms). The addition of oleylamine ligands to the ODE solution of nanocrystals (OLAM:ODE = 60:40), on the other hand, has enabled a rapid growth of CdS nanoparticles causing the average diameter to reach 18.1 nm in just 4 hours. The final product exhibited a narrow size distribution of less than 3%.

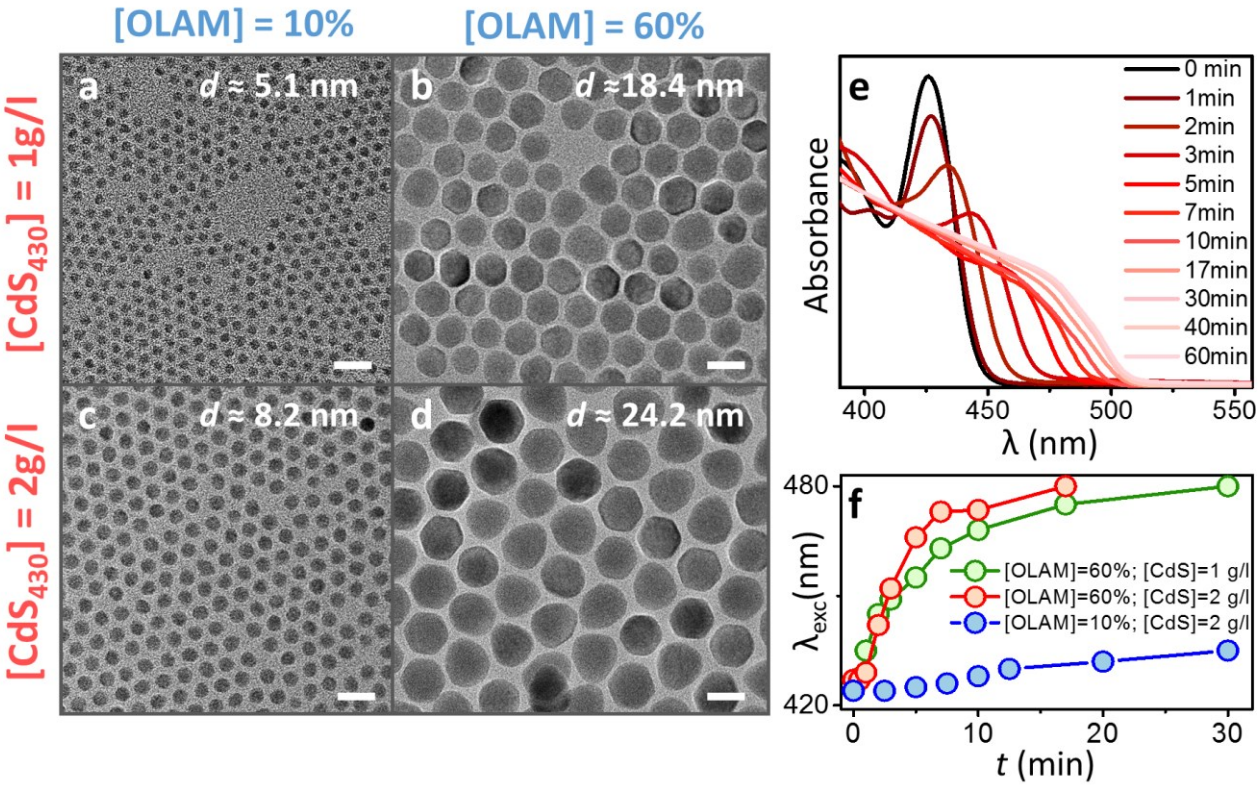

Figure 2. The effect of heating 4.6-nm CdS NCs in a OLAM/ODE mixture for 60 min at T = 260 ˚C. TEM images illustrate the effect of ligand and CdS NC concentrations, [OLAM] and [CdS_{430}], respectively on the ultimate shape of nanocrystals. (a). [OLAM] = 10%, [CdS_{430}] = 1 g/l. (b). [OLAM] = 60%, [CdS_{430}] = 1 g/l. (c). [OLAM] = 10%, [CdS_{430}] = 2 g/l. (d). [OLAM] = 60%, [CdS_{430}] = 2 g/l. The scale bars are 20 nm. (e). The evolution of the CdS NCs absorption

profile resulting from heating of 4.6-nm CdS seeds in 60:40 OLAM:ODE mixture for 60 min. [CdS_{430}] = 2 g/l. (f). The evolution of the exciton absorption in CdS NCs accompanying the digestive ripening process at different reaction conditions.

The particle diameter evolution accompanying the digesting ripening of 4.6-nm CdS NCs were inferred from the absorption profile changes in Fig. 2e. The addition of OLAM ligands to the ODE solution of CdS NCs (OLAM/ODE = 60:40) signified the start of the nanoparticle growth as was evident by the characteristic red-shift of the exciton absorption feature. The growth rate appeared to be dependent both on the ligand concentration and the concentration of CdS seeds. For instance, the 60:40 OLAM/ODE reaction mixture promoted a notably faster CdS particle growth than in the case of 10:90 OLAM/ODE combination, as evident from the TEM size analysis in Figs. 2a-2d and Fig. SF6. Likewise, a greater concentration of CdS seeds has given rise to a product with a relatively larger diameter (Figs. 2a, 2c). Along these lines, 24.2-nm CdS particles could be grown from 4.6-nm CdS seeds *via* the DR process in just 60 min provided that [OLAM] = 60% and [CdS_{430}] = 2 g/l, however, in the case of lower ligand and seed concentrations, [OLAM] = 20% and [CdS_{430}] = 1 g/l, only a moderate increase $d = 4.6 \rightarrow 8.7$ nm was observed after 9 hours of refluxing (see SF2b). In all cases, the dispersion of particle diameters was found to decrease with heating time. Based on averaging the results of several experiments, it was concluded that the CdS nanocrystal growth saturated at $d \approx 25$ nm, regardless of the ligand concentration. Upon reaching this size, the product became prone to precipitation and destabilization, as shown in Fig. SF2a.

Replacing OLAM with oleic acid (OA) as a DR-initiating ligand has produced similar increases in the average nanoparticle size at T = 260 ˚C (see Figs. 3c, 3d) but lead to predominantly cubic shaped nanostructures (Fig. 3d). The splitting of the exciton absorption feature into two was also observed during the OA-initiated DR process (see Figs. 3b and SF3a).[59]

The apparent difference in nanoparticle shapes between OLAM and OA induced ripening, however, were not associated with the difference in the crystalline structure, which, in both cases, was wurtzite (Fig. 3a). Notably, the original CdS seeds inhibited a zinc blende crystal structure (Fig. 3a, red curve), suggesting the DR-triggered phase transition of the CdS lattice.

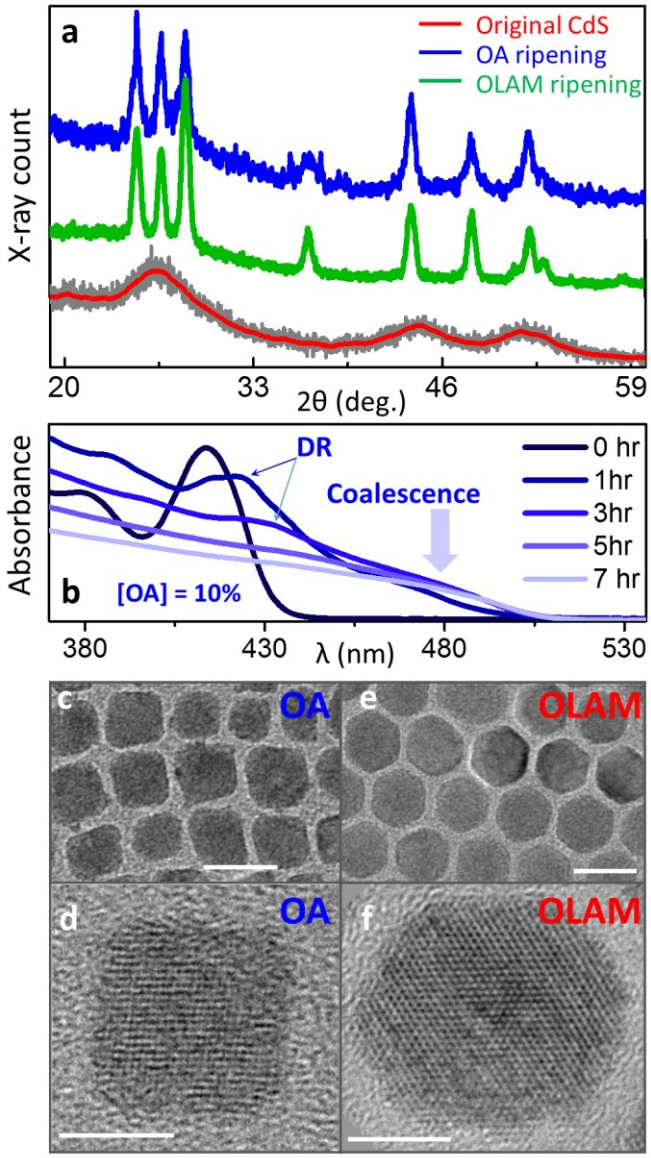

Figure 3. A comparison of the digestive ripening dynamics in oleic acid and oleylamine ligand environments. (a). X-ray powder diffraction analysis of CdS NCs produced through digestive

ripening in OA/ODE = 60:40 (blue) and OLAM/ODE = 60:40 (green) ligand/solvent reaction mixtures. Both structures exhibited a characteristic wurtzite lattice pattern. The Bragg lines of the original 4.4-nm CdS NCs (red) indicated a zinc blende crystal structure. (b). The evolution of the CdS NC absorption profile resulting from digestive ripening in a OA/ODE = 10:90 mixture at T = 260 ˚C. (c, d). TEM images of CdS NCs grown in a OA/ODE = 60:40 mixture for 1 hour. The scale bars are 20 nm and 5 nm in (c) and (d), respectively. (e, f). TEM images of CdS NCs grown in a OLAM/ODE = 60:40 mixture for 1 hour. The scale bars are 20 nm and 5 nm in (e) and (f), respectively.

To explore the key factors contributing to digestive ripening of semiconductor nanocrystals, we have designed a control sample comprising a mixture of small and large diameter CdS NCs. By co-reacting a small amount of 3-nm CdS with larger, 14-nm CdS NCs, we were able to distinguish between three separate growth scenarios: (*i*) – the redissolution of small-diameter nanoparticles in favor of large ones (Ostwald ripening), (*ii*) – the redissolution of larger particles in favor of small ones (conventional DR), and (*iii*) – the interparticle coalescence. Fig. 4b shows the absorbance profile of the (3-nm CdS + 14-nm CdS) nanocrystal mixture. Small-diameter CdS NCs can be identified by a distinguishable excitonic feature at λ = 385 nm, while 14-nm CdS nanostructures give rise to a shoulder-like step at λ = 470 nm. In order to suppress the process of small-to-small particle coalescence, the amount of small-diameter nanoparticles was reduced to yield a minimally observable absorbance feature. Heating the two nanoparticle types in a 60:40 OLAM/ODE ligand/solvent combination promoted a slow growth of CdS_{385} crystallites at temperatures below T = 220 ˚C, as was evident from excitonic the red-shift in Figs. 4c and 4d. At T = 220 ˚C, the nanoparticles growth has accelerated resulting in an

abrupt shift of the excitonic peak from 390 nm to 430 nm (Fig. 4d) followed by either the loss of the quantum confinement or inhomogeneous broadening of this feature at T > 240 ˚C. Importantly, the observed red shifting of the CdS_{385} exciton edge prior to the accelerated growth phase strongly suggests that smaller-diameter dots did not dissolve, such as in the process of Ostwald ripening, but rather grew in size. This behavior is consisted with the conventional DR mechanism, where larger nanoparticles slowly dissolve in favor of smaller ones. The abrupt size increase at T = 220 ˚C could be attributed to either the continuing redissolution of larger particles in favor of small ones (classic digestive ripening) or the attachment of small particles to surfaces of larger ones (coalescence). Out of the two scenarios, the most likely was revealed by TEM images of CdS_{385}-CdS_{470} dimer structures in Fig. 4e showing the attachment of small particles to larger ones during the accelerated particle growth stage, T > 220 ˚C. The continuing red-shifting of the CdS_{470} shoulder accompanying the T = 220-240 ˚C temperature growth corroborates the attachment hypothesis. Consequently, we conclude that the abrupt red-shift of the nanoparticle absorption edge at T = 220 ˚C should be attributed to the particle coalescence. We note that this process is not commonly observed during digestive ripening of metal colloids, as these are typically grown at lower temperatures.

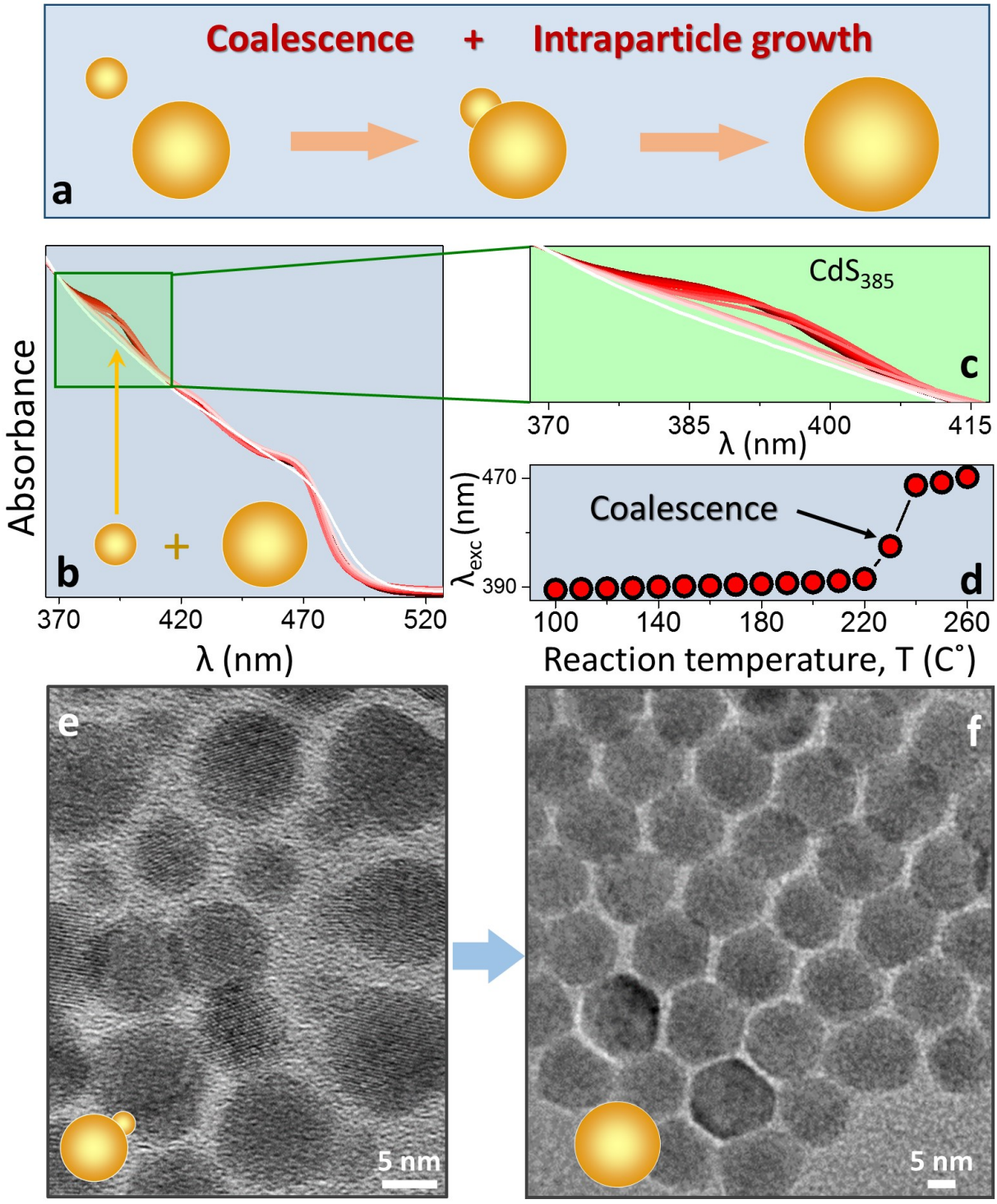

Figure 4. Exploring the mechanism of digestive ripening using a blend of 3-nm and 14-nm CdS nanocrystals in a OLAM/ODE = 60:40 ligand/solvent reaction mixture. (a). The schematics of the observed two-step digestive ripening process, which involves coalescence and intraparticle

growth mechanisms. (b). The evolution of the CdS_{385} + CdS_{470} NC mixture absorption profile during the 1-hour reaction accompanied by the T = 100 → 260 ˚C temperature increase. (c). The magnified portion of the absorption profile in (b) shows the gradual red-shift of the CdS_{385} exciton feature with the reaction temperature. The associated changes in the spectral position of the peak are plotted in (d). (e). TEM evidence of the particle coalescence during digestive ripening. Scale bar is 5 nm. (f). Re-shaping of the coalesced nanoparticle dimers at higher temperatures (T > 240 ˚C) from dimer-like to hexagonal. Scale bar is 5 nm.

The formation of dimer structures during the coalescence stage (Fig. 4e) is eventually followed by the formation of spherical (or hexagonal) nanoparticles with a narrow size distribution (Fig. 4f). This observation suggests that some degree of the intraparticle growth may be contributing at this stage as a mechanism, which transforms the dimers into thermodynamically stable shapes. To test this hypothesis, we have explored the dynamics of digestive ripening in CdS nanorods featuring high energy facets (Fig. 5a). Heating these structures in a 90:10 OLAM:ODE solution resulted in a gradual red-shift of the exciton absorbance reflecting the average diameter increase. TEM images of the DR product confirm the reduction in the aspect ratio of nanorod structures after 30 min of the reaction (Fig. 5b) and the eventual formation of spherical nanoparticles with an average volume being approximately equal to that of original rods (Fig. 5c). Based on these observations, we conclude that the presence of ion solubilizing ligands, in this case, causes some degree of the intraparticle growth, a process which was originally reported for semiconductor colloids by Peng et al.[48]

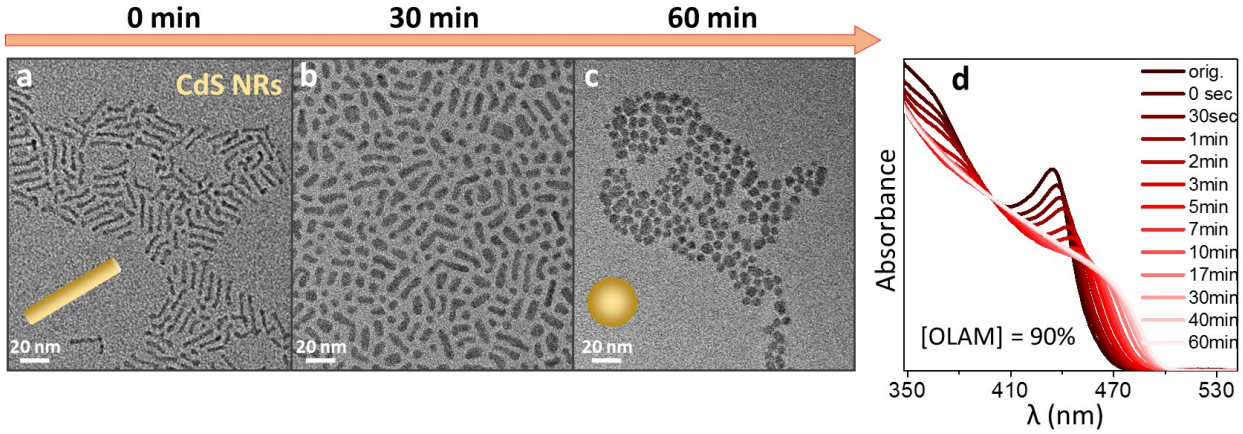

Figure 5. Digestive ripening of CdS semiconductor nanorods *via* the intraparticle growth. (a). TEM image of original CdS nanorods. (b). The product forming after 30 min of digestive ripening at T = 260 ˚C in a 90:10 OLAM/ODE mixture. (c). Spherical nanoparticles form after 60 min of digestive ripening at T = 260 ˚C. (d). The corresponding evolution of the CdS nanorod absorption profile during 60 min of digestive ripening in a 90:10 OLAM/ODE mixture.

The aforementioned experiments imply that the process of digestive ripening in CdS NCs leads to: (*i*) – focusing of nanoparticle sizes towards the average ensemble dimeter at temperatures below the thermal threshold for coalescence, and (*ii*) – coalescence-driven growth of larger diameter structures at higher temperatures. To verify the threshold-like behavior of the DR mechanism in semiconductor NCs, we have explored both low- and high-temperature regimes using two model systems: $CsPbBr_3$ perovskite nanocrystals and large-diameter non-uniform CdS NCs. In both cases, the starting nanoparticles were loaded into a flask containing 60:40 OLAM/ODE mixture and slowly heated up in order to reveal the corresponding shape evolution.

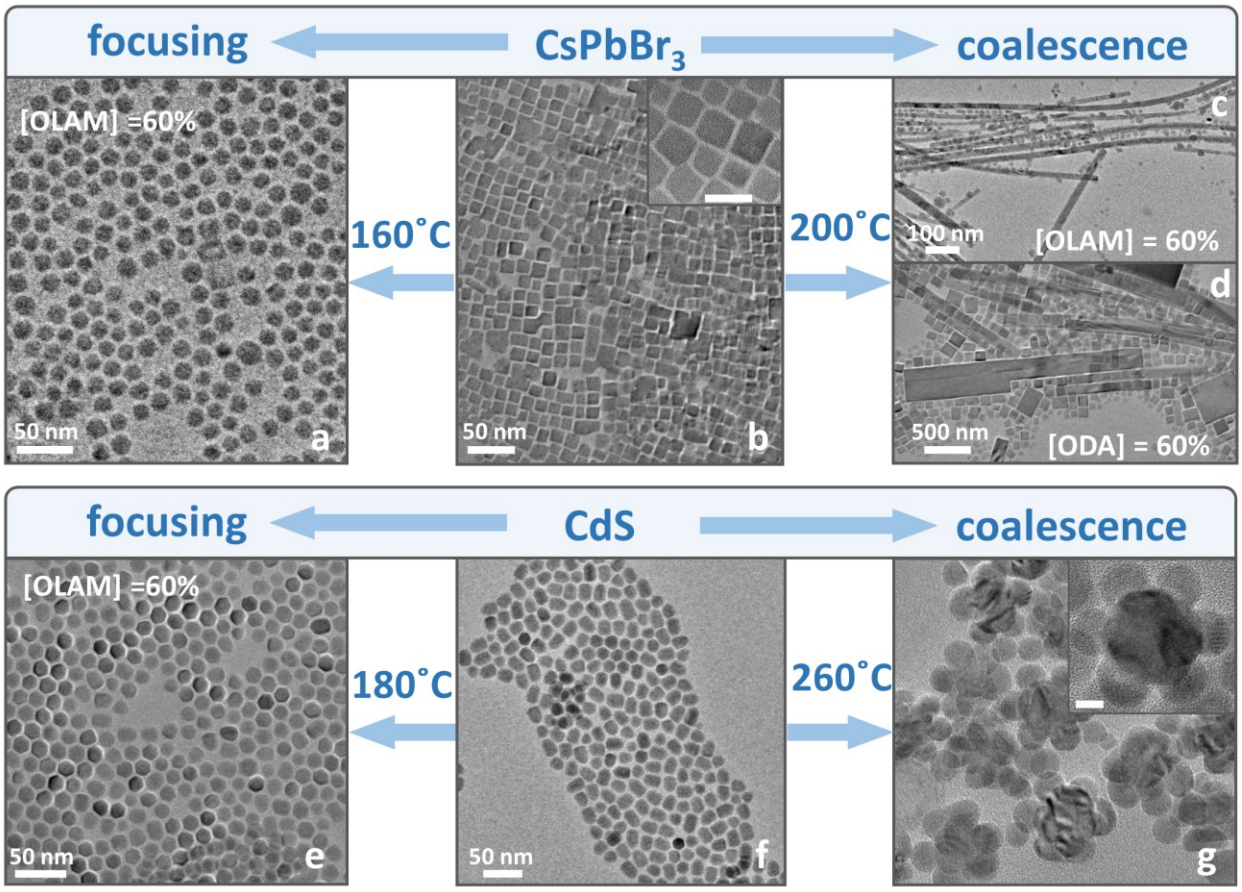

Figure 6. The TEM analysis of the reaction temperature effect on digestive ripening dynamics of $CsPbBr_3$ and CdS NCs. (a). Low-temperature DR of $CsPbBr_3$ NCs in a OLAM:ODE = 60:40 mixture (T = 160 ˚C) preserves the average size of original cubic-shaped $CsPbBr_3$ seeds shown in (b). (c-d). High-temperature digestive ripening of $CsPbBr_3$ NCs (T = 200 ˚C) in the presence of (c) - OLAM and (d) - ODA ligands leads to nanoparticle assembly into ultralong wires and three-dimensional superstructures, respectively, suggesting a significant impact of the interparticle coalescence. (e). Low-temperature DR of CdS NCs in a OLAM:ODE = 60:40 mixture (T = 180 ˚C) preserves the average size of original seeds shown in (f), which is accompanied by the reduction in the size dispersion from 11% to 6%. (h). High-temperature

digestive ripening of CdS NCs (T = 260 ˚C) in the OLAM:ODE = 60:40 mixture leads to nanoparticle coalescence into flower-like superstructures.

According to Fig. 6, the low-temperature DR regime results in the reduction of particle size dispersions for both $CsPbBr_3$ (Fig. 6a) and CdS (Fig. 6e) NCs in comparison with the respective original samples in Figs. 6b and 6f. Interestingly, the morphology of $CsPbBr_3$ NCs has evolved from cubic to nearly spherical without significant changes in the average particle size. In the case of CdS NCs, the original shape dispersion of 11% was reduced to about 6%, consistent with the expected size-focusing effect (see Fig. SF7 for size histograms). In both materials, the low-temperature regime was similar to a classic DR growth, typically observed in metal nanoparticles. At higher DR temperatures, (T_{CdS} = 260 ˚C and $T_{CsPbBr3}$ = 200 ˚C), the particle shape evolution was driven primarily by coalescence, as evident from TEM images in Figs. 6c, 6d, 6g. The samples of coalesced nanoparticles were obtained by stopping the reaction shortly after the maximum temperature was reached in order to minimize the subsequent intraparticle growth. In the case of perovskite nanocrystals, a one-directional assembly of starting cubic seeds into nanowires was observed (Fig. 6c). When ODA molecules were used as DR-initiating ligands, $CsPbBr_3$ nanocrystals were found to form three-dimensional superstructures, as shown in Fig 6d. Evidence of the interparticle coalescence was also observed in the case of CdS NCs that were found to aggregate into flower-shaped structures at T = 260 ˚C (Fig. 6g). This morphology, however, was only reproducible when the original sample contained fairly polydisperse seeds. Overall, the data in Fig. 6 suggests that the DR process in semiconductor nanocrystals exhibits a threshold-like temperature dependence with low-T regime resembling the classical DR process in metal nanoparticles (size focusing towards the ensemble average size)

while the high-T mode promotes interparticle coalescence. The coalesced structures, in the latter case, become more uniform with the extended heating time due to an intraparticle growth (see Fig. 5).

The digestive ripening of 2.7-nm CdSe nanocrystals has resulted in the similar dynamics characterized by size focusing at temperatures below T = 200 ˚C and a significant coalescence at T = 260 ˚C (see Fig. SF3). To further explore the DR growth mechanism, we have looked into a possibility of improving the size dispersion of as prepared $CuZnSnS_4$ colloids. Nanocrystals of this quaternary semiconductor are notoriously difficult to synthesize due to a large spread of particle diameters, providing the additional motivation to use the digestive ripening treatment.

Digestive ripening of $CuZnSnS_4$ NCs was performed starting with highly irregular $CuZnSnS_4$ nanocrystal seeds prepared *via* conventional hot injection routes.[51] The TEM image of original $CuZnSnS_4$ nanoparticles in Fig. 7a shows a broad dispersion of shapes and sizes, consistent with previous reports.[60,61] Following the hot-injection synthesis, as prepared $CuZnSnS_4$ nanocrystals were placed into a 70:30 OLAM/ODE solution and heated up to 260 ˚C for 8 hours. The TEM images of the product at 4 and 8 hours of the reaction show gradual narrowing of the size dispersion with the final product featuring 14 ± 2 nm $CuZnSnS_4$ nanoparticles.

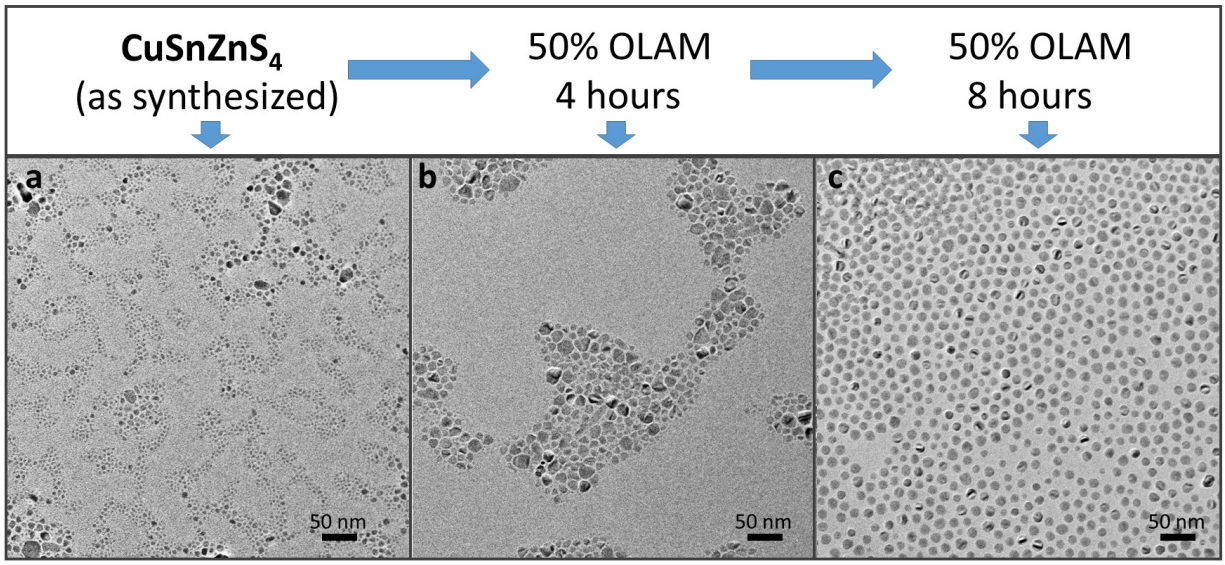

Figure 7. Digestive ripening of $CuZnSnS_4$ nanocrystals. (a). TEM image of original $CuZnSnS_4$ nanocrystal seeds fabricated via hot injection routes. (b). TEM image of $CuZnSnS_4$ nanocrystals after 4 hours of digestive ripening at T = 260 ˚C in a 70:30 OLAM/ODE mixture. (c). TEM image of $CuZnSnS_4$ nanocrystals after 8 hours of digestive ripening at T = 260 ˚C in a 70:30 OLAM/ODE mixture.

CONCLUSIONS

In conclusion, we demonstrate that digestive ripening of semiconductor nanocrystals can be used to control both the particle size and the corresponding size dispersion. In contrast to the well-studied ripening mechanism in metal nanoparticles, the digestive ripening of semiconductor nanocrystals leads to significant changes in the average particle diameter at reaction temperatures above a certain thermal threshold. Meanwhile, at low temperatures, size focusing leading to an ensemble average diameter was observed. The existence of a thermal threshold for a particle coalescence allowed controlling the ultimate size of semiconductor nanocrystals through the DR

approach, a functionally, which is not easily accessible in the DR treatment of metal nanoparticles. The ability to tune nanoparticle diameter while reducing the size dispersion has been demonstrated for samples of CdS, CdSe, $CsPbBr_3$, and $CuSnZnS_4$ semiconductor colloids. We expect that the DR approach could be extended to other semiconductor materials as a simple tool for advanced shape control of colloidal nanostructures.

Supporting information. Experimental section, additional figures and details of calculation. This material is available free of charge via the Internet at http://pubs.acs.org.

Acknowledgment. We gratefully acknowledge NSF Award DMR-1710063 for financial support. PG was funded by the Welch foundation grant # U-0047. PM was supported in part by CHE-1465052 Award.

REFERENCES

[1] Murray, C. B.; Norris, D. J.; Bawendi, M. G. Synthesis and Characterization of Nearly Monodisperse CdE (E = Sulfur, Selenium, Tellurium) Semiconductor Nanocrystallites. *J. Am. Chem. Soc.* **1993**, *115*, 8706–8715.

[2] Kovalenko, M. V.; Manna, L.; Cabot, A.; Hens, Z.; Talapin, D. V.; Kagan, C. R.; Klimov, V. I.; Rogach, A. L.; Reiss, P.; Milliron, D. J.; Guyot-Sionnnest, P.; Konstantatos, G.; Parak, W.J.; Hyeon, T.; Korgel, B. A.; Murray, C. B.; Heiss, W. Prospects of Nanoscience with Nanocrystals. *ACS Nano*, **2015**, *9*, 1012–1057.

[3] Reiss P. Synthesis of Semiconductor Nanocrystals in Organic Solvents. In: *Semiconductor Nanocrystal Quantum Dots: Synthesis, Assembly, Spectroscopy and Applications*; Rogach, A. L., Ed., Springer: Wien-New York; 2008, pp. 35-72.

[4] Peng, X. G.; Wickham, J.; Alivisatos, A. P. Kinetics of II-VI and III-V Colloidal Semiconductor Nanocrystal Growth: "Focusing" of Size Distributions. *J. Am. Chem. Soc.* **1998**, *120*, 5343-5344.

[5] Dai, Q.; Wang, Y.; Li, X.; Zhang, Y.; Pellegrino, D. J.; Zhao, M.; Zou, B.; Seo, J.; Wang, Y.; Yu, W. W. Size-Dependent Composition and Molar Extinction Coefficient of PbSe Semiconductor Nanocrystals. *ACS Nano* **2009**, *3*, 1518−1524.

[6] Chen, O.; Yang, Y. A.; Wang, T.; Wu, H. M.; Niu, C. G.; Yang, J. H.; Cao, Y. C. Surface-Functionalization-Dependent Optical Properties of II-VI Semiconductor Nanocrystals. *J. Am. Chem. Soc.* **2011**, *133*, 17504−17512.

[7] Talapin, D. V.; Rogach, A. L.; Kornowski, A.; Haase, M.; Weller, H. Highly Luminescent Monodisperse CdSe and CdSe/ZnS Nanocrystals Synthesized in a Hexadecylamine-Trioctylphosphine Oxide-Trioctylphospine Mixture. *Nano Lett.* **2001**, *1*, 207–211.

[8] Hines, M. A.; Scholes, G. D. Colloidal PbS Nanocrystals with Size-Tunable Near-Infrared Emission: Observation of Post-Synthesis Self-Narrowing of the Particle Size Distribution. *Adv. Mater.* **2003**, *15*, 1844–1849.

[9] Donega, C. D.; Hickey, S. G.; Wuister, S. F.; Vanmaekelbergh, D.; Meijerink, A. Single-Step Synthesis to Control the Photoluminescence Quantum Yield and Size Dispersion of CdSe Nanocrystals. *J. Phys. Chem. B* **2003**, *107*, 489−496.

[10] Greytak, A. B.; Tan, R.; Roberts, S. K. Prospects for Rational Control of Nanocrystal Shape Through Successive Ionic Layer Adsorption and Reaction (SILAR) and Related Approaches. In: *Anisotropic and Shape-Selective Nanomaterials. Nanostructure Science and Technology*; Hunyadi Murph, S. E.; Larsen, G.; Coopersmith, K., Eds. Springer: Cham, Switzerland; 2017, pp. 169-232.

[11] Boles, M. A.; Engel, M.; Talapin, D. V. Self-Assembly of Colloidal Nanocrystals: From Intricate Structures to Functional Materials. *Chem. Rev.* **2016**, *116*, 11220-11289.

[12] Chandler, R. E.; Houtepen, A. J.; Nelson, J.; Vanmaekelbergh, D. Electron Transport in Quantum Dot Solids: Monte Carlo Simulations of the Effects of Shell Filling, Coulomb Repulsions, and Site Disorder. *Phys. Rev. B* **2007**, *75*, 085325.

[13] Mashford, B. S.; Stevenson, M.; Popovic, Z.; Hamilton, C.; Zhou, Z.; Breen, C.; Steckel, J.; Bulovic, V.; Bawendi, M. G.; Coe-Sullivan S.; Kazlas, P. T. High-Efficiency Quantum-Dot Light-Emitting Devices with Enhanced Charge Injection. *Nat. Photonics* **2013**, *7*, 407-412.

[14] Empedocles, S. A.; Neuhauser, R.; Shimizu, K.; Bawendi, M. G. Photoluminescence from Single Semiconductor Nanostructures. *Adv. Mater.* **1999**, *11*, 1243-1256.

[15] Kholmicheva, N.; Moroz, P.; Bastola, E.; Razgoniaeva, N.; Bocanegra, J.; Shaughnessy, M.; Porach, Z.; Khon, D.; Zamkov, M. Mapping the Exciton Diffusion in Semiconductor Nanocrystal Solids. *ACS Nano* **2015**, *9*, 2926-2937.

[16] Choi, J. J.; Luria, J.; Hyun, B. R.; Bartnik, A. C.; Sun, L.; Lim, Y. F.; Marohn, J. A.; Wise, F. W.; Hanrath, T. Photogenerated Exciton Dissociation in Highly Coupled Lead Salt Nanocrystal Assemblies. *Nano Lett.* **2010**, *10*, 1805–1811.

[17] Zhitomirsky, D.; Voznyy, O.; Hoogland, S.; Sargent, E. H. Measuring Charge Carrier Diffusion in Coupled Colloidal Quantum Dot Solids. *ACS Nano* **2013**, *7*, 5282-5290.

[18] Talapin, D. V.; Shevchenko, E. V.; Bodnarchuk, M. I.; Ye, X.; Chen, J.; Murray, C. B. Quasicrystalline Order in Self-Assembled Binary Nanoparticle Superlattices. *Nature* **2009**, *461*, 964–967

[19] LaMer, V. K.; Dinegar, R. H. Theory, Production and Mechanism of Formation of Monodispersed Hydrosols. *J. Am. Chem. Soc.* **1950**, *72*, 4847−4854.

[20] Chu, D. B. K.; Owen, J. S.; Peters, B. Nucleation and Growth Kinetics from LaMer Burst Data. *J. Phys. Chem. A*, **2017**, *121*, 7511–7517

[21] Hendricks, M. P.; Campos, M. P.; Cleveland, G. T.; Jen-La Plante, I.; Owen, J. S. A Tunable Library of Substituted Thiourea Precursors to Metal Sulfide Nanocrystals. *Science* **2015**, *348*, 1226-1230.

[22] Clark, M. D.; Kumar, S. K.; Owen, J. S.; Chan, E. M. Focusing Nanocrystal Size Distributions via Production Control. *Nano Lett.* **2011**, *11*, 1976–1980.

[23] Chemseddine, A.; Weller, H. Highly Monodisperse Quantum Sized CdS Particles by Size Selective Precipitation. *Ber. Bunsenges. Phys. Chem.* **1993**, *97*, 636–638.

[24] Vossmeyer, T; Katsikas, L; Giersig, M; Popovic, I. G.; Chemseddine, A.; Eychmueller, A.; Weller, H. CdS Nanoclusters - Synthesis, Characterization, Size-Dependent Oscillator Strength,

Temperature Shift of The Excitonic-Transition Energy, and Reversible Absorbency Shift. *J. Phys. Chem.*, **1994**, *98*, 7665–7673.

[25] Yin, Y.; Alivisatos, A. P. Colloidal Nanocrystal Synthesis and the Organic–Inorganic Interface. *Nature* **2005**, *437*, 664-670.

[26] Rempel, J. Y., Bawendi, M. G., Jensen, K. F. Insights into the Kinetics of Semiconductor Nanocrystal Nucleation and Growth. *J. Am. Chem. Soc.* **2009**, *131*, 4479–4489.

[27] Van Embden, J.; Chesman, A. S. R.; Jasieniak, J. J. The Heat-Up Synthesis of Colloidal Nanocrystals. *Chem. Mater.* **2015**, *27*, 2246–2285

[28] Liu, H.; Owen, J. S.; Alivisatos, A. P. Mechanistic Study of Precursor Evolution in Colloidal Group II-VI Semiconductor Nanocrystal Synthesis. *J. Am. Chem. Soc.* **2007**, *129*, 305–312.

[29] Zhuang, Z.; Peng, Q.; Li, Y. Controlled Synthesis of Semiconductor Nanostructures in the Liquid Phase. *Chem. Soc. Rev.* **2011**, *40*, 5492−5513.

[30] García-Rodríguez, R.; Hendricks, M. P.; Cossairt, B.M.; Liu, H.; Owen, J. S. Conversion Reactions of Cadmium Chalcogenide Nanocrystal Precursors. *Chem. Mater.* **2013**, *25*, 1233−1249.

[31] Thanh, N. T. K.; Maclean, N.; Mahiddine, S. Mechanisms of Nucleation and Growth of Nanoparticles in Solution *Chem. Rev.* **2014**, *114*, 7610–7630.

[32] Abe, S.; Čapek, R. K.; De Geyter, B.; Hens, Z. Tuning the Postfocused Size of Colloidal Nanocrystals by the Reaction Rate: From Theory to Application. *ACS Nano*, **2012**, *6*, 42–53.

[33] Razgoniaeva, N.; Carrillo, L.; Burchfield, D.; Moroz, P.; Adhikari, P.; Yadav, P.; Khon, D.; Zamkov, M. Colloidal Synthesis of Monodisperse Semiconductor Nanocrystals through the Saturated Ionic Layer Adsorption. *Chem. Mater.* **2016**, *28*, 2823-2833.

[34] Ithurria, S.; Talapin, D. V. Colloidal Atomic Layer Deposition (c-ALD) using Self-Limiting Reactions at Nanocrystal Surface Coupled to Phase Transfer between Polar and Nonpolar Media. *J. Am. Chem. Soc.* **2012**, *134*, 18585−18590.

[35] Lin, X. M.; Sorensen, C. M.; Klabunde, K. J. Digestive Ripening, Nanophase Segregation and Superlattice Formation in Gold Nanocrystal Colloids. *J. Nanopart. Res.* **2000**, *2*, 157−164.

[36] Lee, W.; Kim, M. G.; Choi, J.-R.; Park, J.-I.; Ko, S. J.; Oh, S. J.; Cheon, J. Redox−Transmetalation Process as a Generalized Synthetic Strategy for Core−Shell Magnetic Nanoparticles. *J. Am. Chem. Soc.* **2005**, *127*, 16090-16097

[37] Lee, D.-K.; Park, S.-I.; Lee, J. K.; Hwang, N.-M. A Theoretical Model for Digestive Ripening. *Acta Mater.* **2007**, *55*, 5281−5288.

[38] Ostwald, W. Z. Ostwald Ripening Theory. *Phys. Chem.* **1900**, *34*, 495.

[39] Polte, J.; Ahner, T. T.; Delissen, F.; Sokolov, S.; Emmerling, F.; Thunemann, A. F.; Kraehnert, R. Mechanism of Gold Nanoparticle Formation in the Classical Citrate Synthesis Method Derived from Coupled In Situ XANES and SAXS Evaluation. *J. Am. Chem. Soc.* **2010**, *132*, 1296-1301.

[40] Sahu, P.; Prasad, B. L. V. Fine Control of Nanoparticle Sizes and Size Distributions: Temperature and Ligand Effects on the Digestive Ripening Process. *Nanoscale* **2013**, *5*, 1768−1771.

[41] Wang, J.; Boelens, H. F. M.; Thathagar, M. B.; Rothenberg, G. *In Situ* Spectroscopic Analysis of Nanocluster Formation. *ChemPhysChem* **2004**, *5*, 93-98.

[42] Nishimura, S.; Takagaki, A.; Maenosono, S.; Ebitani, K. *In Situ* Time-Resolved XAFS Study on the Formation Mechanism of Cu Nanoparticles Using Poly(N-vinyl-2-pyrrolidone) as a Capping Agent. *Langmuir* **2009**, *26*, 4473-4479.

[43] Seth, J.; Prasad, B. L. V. Bromide Ion Mediated Modification to Digestive Ripening Process: Preparation of Ultra-Small Pd, Pt, Rh and Ru Nanoparticles. *Nano Res.* **2016**, *9*, 2007-2017.

[44] Casula, M. F.; Jun, Y.-w.; Zaziski, D. J.; Chan, E. M.; Corrias, A.; Alivisatos, A. P. The Concept of Delayed Nucleation in Nanocrystal Growth Demonstrated for the Case of Iron Oxide Nanodisks. *J. Am. Chem. Soc.* **2006**, *128*, 1675-1682.

[45] Kudera, S.; Zanella, M.; Giannini, C.; Rizzo, A.; Li, Y.; Gigli, G.; Cingolani, R.; Ciccarella, G.; Spahl, W.; Parak, W.; Manna, L. Sequential Growth of Magic-Size CdSe Nanocrystals. *Adv. Mater.* **2007**, *19*, 548-552.

[46] Cingarapu, S.; Yang, Z.; Sorensen, C. M.; Klabunde, K. J. Synthesis of CdSe/ZnS and CdTe/ZnS quantum dots: refined digestive ripening. *J. Nanomater.* **2012**, *312087*, 1−12.

[47] Cingarapu, S.; Yang, Z.; Sorensen, C. M.; Klabunde, K. J. Synthesis of CdSe Quantum Dots by Evaporation of Bulk CdSe using SMAD and Digestive Ripening Processes. *Chem. Mater*. **2009**, *21*, 1248−1252

[48] Peng, X.; Manna, L.; Yang, W.; Wickham, J.; Scher, E.; Kadavanich, A.; Alivisatos, A. P. Shape control of CdSe nanocrystals. *Nature* **2000**, *404*, 59-61.

[49] Shimpi, J. R.; Sidhaye, D. S.; Prasad, B. L. V. Digestive Ripening: A Fine Chemical Machining Process on the Nanoscale. *Langmuir* **2017**, *33*, 9491-9507.

[50] Razgoniaeva, N.; Moroz, P.; Yang, M.; Budkina D. S.; Eckard, H.; Augspurger, M.; Khon, D.; Tarnovsky, A. N.; Zamkov, M. One-Dimensional Carrier Confinement in "Giant" CdS/CdSe Excitonic Nanoshells *J. Am. Chem. Soc.* **2017**, *139*, 7815–7822

[51] Collord, A. D.; Hillhouse, H. W. Composition Control and Formation Pathway of CZTS and CZTGS Nanocrystal Inks for Kesterite Solar Cells. *Chem. Mater.* **2015**, *27*, 1855−1862

[52] Peng, Z. A.; Peng, X. G. Nearly Monodisperse and Shape-Controlled CdSe Nanocrystals via Alternative Routes: Nucleation and Growth. *J. Am. Chem. Soc.* **2002**, *124*, 3343-3353.

[53] Protesescu, L.; Yakunin, S.; Bodnarchuk, M. I.; Krieg, F.; Caputo, R.; Hendon, C. H.; Yang, R. X.; Walsh, A.; Kovalenko, M. V. Nanocrystals of Cesium Lead Halide Perovskites (CsPbX3, X = Cl, Br, and I): Novel Optoelectronic Materials Showing Bright Emission with Wide Color Gamut. *Nano Lett.* **2015**, *15*, 3692−3696.

[54] Buffat, P.; Borel, J. P. Size effect on the melting temperature of gold particles. *Phys. Rev. A: At., Mol., Opt. Phys.* **1976**, *13*, 2287-2298.

[55] Jadzinsky, P. D.; Calero, G.; Ackerson, C. J.; Bushnell, D. A.; Kornberg, R. D. Structure of a Thiol Monolayer-Protected Gold Nanoparticle at 1.1 Å Resolution. *Science* **2007**, *318*, 430−433

[56] Hakkinen, H. The Gold-Sulfur Interface at the Nanoscale. *Nat. Chem.* **2012**, *4*, 443-455.

[57] Biener, M. M.; Biener, J.; Friend, C. M. Revisiting the S−Au(111) Interaction: Static or Dynamic? *Langmuir* **2005**, *21*, 1668−1671.

[58] Sahu, P.; Prasad, B. L. V. Time and Temperature Effects on the Digestive Ripening of Gold Nanoparticles: Is There a Crossover from Digestive Ripening to Ostwald Ripening? *Langmuir* **2014**, *30*, 10143-10150.

[59] Scholes, G. D. Controlling the Optical Properties of Inorganic Nanoparticles. *Adv. Funct. Mater.* **2008**, *18*, 1157–1172

[60] Riha, S. C.; Parkinson, B. A.; Prieto, A. L. Solution-Based Synthesis and Characterization of Cu_2ZnSnS_4 Nanocrystals. *J. Am. Chem. Soc.* **2009**, *131*, 12554–12555.

[61] Korala, L.; Braun, M. B.; Kephart, J. M.; Tregillus, Z.; Prieto, A. L. Ligand-Exchanged CZTS Nanocrystal Thin Films: Does Nanocrystal Surface Passivation Effectively Improve Photovoltaic Performance? *Chem. Mater.* **2017**, *29*, 6621−6629